Spectrochimica Acta Part A: Molecular and Biomolecular Spectroscopy 291 (2023) 122297

Contents lists available at ScienceDirect

Spectrochimica Acta Part A:
Molecular and Biomolecular Spectroscopy

journal homepage: www.journals.elsevier.com/spectrochimica-acta-part-a-molecular-and-biomolecular-spectroscopy

Physiochemical characterization of sodium doped zinc oxide nano powder for antimicrobial applications

B. Nageswara Rao [a,b,f], P. Tirupathi Rao [a], K. Vasudha [c], Sk. Esub Basha [a], D.S.L. Prasanna [d,g], T. Bhushana Rao [e], K. Samatha [b], R.K. Ramachandra [a,e,*]

[a] Crystal Growth and Nano-Science Research Center, Department of Physics, Government College (A), Rajamahendravaram, Andhra Pradesh 533105, India
[b] Department of Physics, Andhra University, Visakhapatnam, Andhra Pradesh 530003, India
[c] Department of Biotechnology, Government College (A), Rajamahendravaram, Andhra Pradesh 533105, India
[d] Department of Chemistry, Acharya Nagarjuna University, Guntur 522510, A.P., India
[e] Government Degree College, Chodavaram, Visakhapatnam, Andhra Pradesh 531036, India
[f] Department of Physics, Dr VS Krishna Government Degree College (A), Visakhapatnam, A.P, India
[g] Department of Chemistry, Dr VS Krishna Government Degree College (A), Visakhapatnam, A.P, India

HIGHLIGHTS

- This article reported the synthesis of pure and Na doped zinc oxide nano powders ($Zn_{1-x}Na_xO$) through co-precipitation process.
- Hexagonal wurtzite $Zn_{1-x}Na_xO$ nano powders with high crystallinity and stability were confirmed by XRD.
- The factors such as particle size and surface morphology were controlled with varying Na concentrations.
- The absorption peaks of as-synthesized $Zn_{0.99}Na_{0.01}O$ samples are recorded at 196, 284 and 365 nm, respectively.
- The as-prepared $Zn_{1-x}Na_xO$ nano powders were proved to be excellent antibacterial and antifungal agents.

GRAPHICAL ABSTRACT

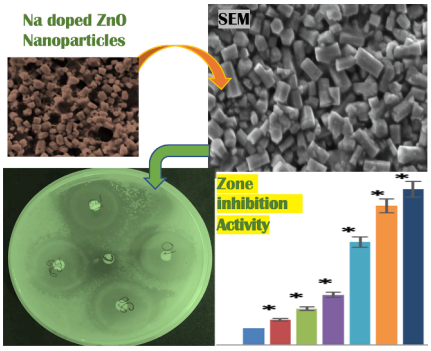

ARTICLE INFO

Keywords:
ZnO NPs
Semiconductors
Optical properties
Antibacterial activity
Antifungal activity

ABSTRACT

Zinc oxide (ZnO) is one of the semiconductor materials with unique antimicrobial properties towards various microorganisms. In this article, pure and Na doped ZnO nanopowders were synthesized by easiest and cost-effective co-precipitation process. X-ray diffraction (XRD), Fourier transform infrared spectroscopy (FT-IR), ultraviolet – visible (UV – Vis) spectroscopy, scanning electron microscopy (SEM), and Energy dispersive X-ray analysis (EDAX) techniques were used to characterize the particle size, surface morphology and chemical composition of prepared materials. The XRD analysis revealed that the samples exhibiting hexagonal wurtzite crystal structure with high crystallinity and the average crystallite size values increased from 23.51 to 28.118 nm. The UV – Vis spectroscopy results exposed that the bandgap energy (E_g) of the samples with the values in the range of 3.068–3.301 eV. The SEM micrographs showed that the morphology of the of synthesized particles are hexagonal and spherical in nanometric size. The EDX spectra confirmed the elemental composition of Na, Zn and O in the crystal lattice and FTIR spectroscopic data proved the formation of functional groups and the presence of

* Corresponding author.
E-mail address: ramc@gcrjy.ac.in (R.K. Ramachandra).

https://doi.org/10.1016/j.saa.2022.122297
Received 9 November 2022; Received in revised form 23 December 2022; Accepted 28 December 2022
Available online 31 December 2022
1386-1425/© 2022 Elsevier B.V. All rights reserved.

chemical bonding at the ZnO interface. Antibacterial activity of pure and Na doped Zinc oxide nanoparticles against Gram-negative pathogens such as Escherichia coli, Pseudomonas aeruginosa & Klebsiella pneumoniae and Gram-positive pathogens such as *Staphylococcus aureus* reveal that the zone of inhibition increases with increasing Na concentration. The antifungal activity against *Aspergillus* and *Candida* was investigated. These results demonstrated that the pure and Na doped ZnO samples exhibit enhanced antibacterial and antifungal activity with increasing particle size in presence of visible light and they could be used as good antibacterial as well as antifungal agents.

1. Introduction

Semiconductor nanomaterials with large band gap have drawn much interest to the researchers in the field of electronics, optics, optoelectronics and photovoltaic cells. Amongst the various semiconductor nanoparticles discussed so far, Zinc Oxide is a II-VI group compound direct band gap semiconductor with E_g of 3.37 eV and has an exciton binding energy of 60 meV both at room temperature and crystallizes into hexagonal wurtzite structure. It has the ability to grow single crystals as well as high piezoelectricity and exhibit excellent photonic and electrochemical properties [1–3]. Due to these aspects of ZnO, it has been considered to be an important material for various applications ranging from optical sensors, UV laser diodes and nanotechnology-based devices such as plasma displays. Also, nano-powdered ZnO semiconductors have received broad attention because of its applications in the field of electrostatic dissipative coatings, transparent ulta-violet protection films, sensors, spintronic machinery, luminescence, optoelectronics, photocatalysis, varistors, laser technology, imaging, energy conversion, and communications to biotechnology etc. It is a unique material and has a diverse form of growth morphologies, such as nano-rods, nano-bars, nano-rings, nano-springs, stone shaped like nano-structures, nano-belts, nano-wires and nano-cages [4,5].

In recent times, much attention has been given on the synthesis process to produce pure and doped ZnO nanomaterials. ZnO is visible light transparent material and can be improved its conductivity by doping as the dopants have strong influence on the properties of ZnO such as the electrical, optical and optoelectronic properties. In addition, the average crystalline size (D), band gap (E_g) and optical properties of ZnO are improved by introducing dopants into Zinc Oxide matrix. The ZnO doped with various metals (Al, Co, Cd, Eu, Cu, Ni, Ag, Co) show improved properties, since these metals have ionic radius almost matches well with Zn^{2+} (0.74 Å) [6]. Over the last few years, many researchers reported the incorporation of second element into ZnO matrix leads to modify physical and chemical properties. Few of them reported are ZnO:Na [4], ZnO:Ga [5], ZnO:Al [6,7], ZnO:Cd [8], ZnO:Co [9], ZnO:Cr [10], ZnO:Cu [11], ZnO:Eu [12], ZnO:Fe [13], ZnO:In [14], ZnO:Li [15], ZnO:Mn, Fe [16], ZnO:Ni, Al [17], etc. Here, to obtain stable p-type ZnO semiconductor nanopowders, Column-IA (Li, Na, K) and Column-V (P, As, Sb) elements are needed to dope, since these elements acts as deep acceptors or interstitial donors that contribute p-type conductivity [3,18]. In the last few decades, a group of methods have been successfully used for the synthesis of pure and doped Zinc Oxide NPs, such as sol - gel, co-precipitation, solid state reaction method, thermal diffusion method and mild and simple solution method.

During the past few years, many researchers have published their findings on antimicrobial activities of pure and doped zinc oxide nanomaterials and showing that these nanostructures are acted as powerful antibacterial and antifungal agents. According to our literature, the antimicrobial activities of the Na doped ZnO ($Zn_{1-x}Na_xO$) towards various filamentous bacteria and fungi have been rarely reported. Four bacterial strains, Escherichia coli, Pseudomonas aeruginosa, Klebsiella pneumoniae and *Staphylococcus aureus* as well as two fungal pathogens, *Aspergillus* and *Candida* were used against pure and Na doped ZnO samples. However, to best of our knowledge, there is no study reported in the literature particularly for these selected bacterial and fungal strains. In the present paper, the research study demonstrates about synthesis of pure and Na doped ZnO nanoparticles by the simple, low cost and energy consumption effective co-precipitation method. We also studied the structural, morphological, optical, antibacterial, and antifungal properties of pure and Na doped ZnO samples [19,20].

2. Experimental

2.1. Chemicals used

Zinc acetate dihydrate [$Zn(CH_3COO)_2{\cdot}2H_2O$, SRL chem. 99.5%] was used as the starting material for ZnO. Sodium nitrate [$NaNO_3$, Merck Ltd., 99.0%] was used as the source compound for doping with sodium. Sodium hydroxide pellets GR [NaOH, Loba Chemie, 98.0%] was used as an agent. All precursors are used without any further purification as they received.

2.2. Synthesis of the samples

ZnO nanostructures were successfully synthesized in an aqueous medium by taking zinc acetate dihydrate [$Zn(CH_3COO)_2{\cdot}2H_2O$] and sodium hydroxide [NaOH] in a stoichiometric ratio according to the following chemical reactions (1), (2) and the formed sodium salt CH_3COONa has been removed by deionized water [21]:

$$Zn(CH_3COO)_2.2H_2O + NaOH \rightarrow Zn(CH_3COO)(OH) + CH_3COONa(\downarrow) \quad (1)$$

$$Zn(CH_3COO)\ (OH) + NaOH \rightarrow ZnO + CH_3COONa(\downarrow)\ + H_2O \quad (2)$$

The washing process was repeated until the pH of the solution was 7. For the synthesis of pure and sodium doped ZnO nano powders, Zinc acetate dihydrate [$Zn(CH_3COO)_2{\cdot}2H_2O$], sodium nitrate [$NaNO_3$] and sodium hydroxide [NaOH] were used as precursors. During the synthesis of pure and sodium doped ZnO nanoparticles the main parameters such as, particle size, morphology, chemical composition and crystalline structure must be controlled [22]. Sodium doped zinc oxide nanostructures have been prepared by co-precipitation process and the synthesis procedure was shown in the Fig. 1**.** In this synthesis process, 21.95 g of $Zn(CH_3COO)_2{\cdot}2H_2O$ was dissolved in 100 ml of distilled water in a glass beaker and stirred for 30 min using magnetic stirrer. After stirring at room temperature, an appropriate amount of sodium nitrate ($NaNO_3$) solution was prepared and added it to $Zn(CH_3COO)_2{\cdot}2H_2O$ solution. Subsequently, 8 g of NaOH solution was prepared by using 100 ml of deionized water in a separate glass beaker and stirred it for 10 min. Now, this NaOH solution was slowly added drop by drop to the Zn $(CH_3COO)_2{\cdot}2H_2O$ and $NaNO_3$ mixture solution under stirring condition. The suspension formed with the dropping of NaOH alkaline aqueous solution to the $Zn(CH_3COO)_2{\cdot}2H_2O$ and $NaNO_3$ mixture solution and it was magnetic stirred for two hours at the room temperature. Now, the liquid white gel was formed under normal air condition, and it was vacuum filtered using membrane filtration assembly. The solid white gel was formed after vacuum filtration; it was heated in oven at 95 °C for 5 h to get Na-doped ZnO as white nano powders. Different masses of Sodium nitrate were mixed with the mixture of Zinc acetate and NaOH to vary the doping percentage (Na/Na + Zn).

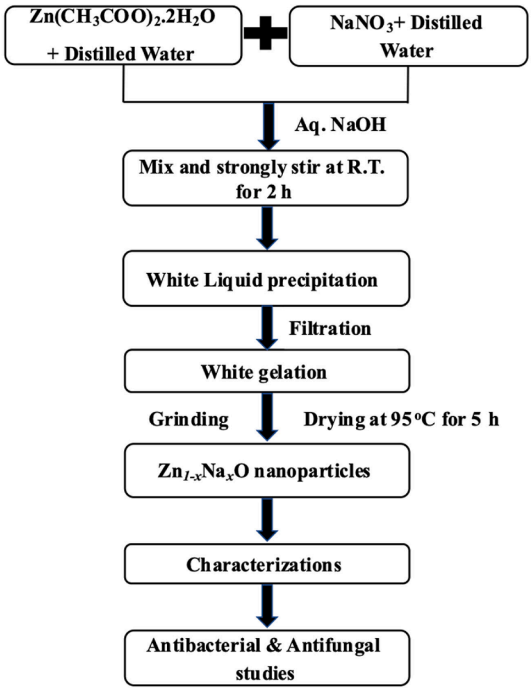

Fig. 1. Flow chart of the co-precipitation synthesis process of sodium doped zinc oxide nanopowders.

2.3. Instrumentation

$Zn_{1-x}Na_xO$ nanopowder samples were characterized by the powder XRD patterns recorded using a Bruker-D8 advance powder x-ray diffractometer with CuK_α radiation and a graphite monochromator in the angle (2θ) range of 30–80°. UV–Visible optical absorption studies for the optical transmission and absorption measurements were carried out for pure and Na doped ZnO nanopowders by Shimadzu UV-1601 spectrometer in the wavelength range of 200–800 cm. Fourier transform infrared spectroscopy was performed to identify the functional groups, which in turn determines the molecular structure of the synthesized nanopowders recorded using Varian-660 FTIR spectrometer in the wave number range of 400–4000 cm^{-1}. Scanning Electron Microscope with High-resolution provides detailed surface data of powder samples, which includes morphological structures, topographical structures and compositional information. For the purpose of these measurements, the powers were ultrasonically dispersed in alcohol and the suspension was deposited on the sample holder. Energy dispersive X-ray spectroscopy for elemental composition of the as-prepared samples was investigated by using EDX analysis.

2.4. Antimicrobial activity test

ZnO nanoparticles were reported as a superior antimicrobial agents and the performance was size and shape-dependent for many nanoparticles, the smaller the size the higher the activity due to their higher specific surface area [23]. However, the ZnO NPs shows strong inhibited fungal and bacterial growth at higher doping concentrations of Na. In the current paper, we reported four types of bacterial cultures and two standard fungal pathogens for $Zn_{1-x}Na_xO$ nanopowders with increased sodium dopant concentrations ($x = 0$, 0.01, 0.02, 0.04, 0.06, 0.08, and 0.10) for their antibacterial activity and antifungal effect, respectively. The bactericidal assay on one strain of Gram-positive Staphylococcus aureus and, three strain of Gram-negative bacteria Pseudomonas aeruginosa, Escherichia coli and Klebsiella pneumoniae was performed. In addition, the antifungal activities of as-synthesized samples towards the economically important fungi, Aspergillus and Candida have been studied.

The Kirby–Bauer disk diffusion method [24] was employed for evaluating antimicrobial activity. For screening antibacterial, antifungal activity nutrient agar medium and potato dextrose agar medium were prepared and sterilized by using autoclave at 121 °C and 15 lbs pressure for 15 to 20 min. The molten agar was poured into sterile Petri plates and allowed to solidify [25]. The 24 hrs old actively growing selected bacterial and fungal cultures were spread on solid nutrient agar plates and on PDA plates. Concurrently, sterilized Whatman filter paper disks of around 6–8 mm size were coated with the graded concentrations of Na-doped ZnO nanoparticle solution and carefully placed on the culture. The plates containing bacterial culture were incubated at 37 °C for 24 hrs and fungal cultures were incubated at 24 °C for 48 hrs.

The antimicrobial activity of the as-synthesized $Zn_{1-x}Na_xO$ nanopowders against all pathogenic microorganisms was studied in terms of zone of inhibition [26]. The zone of inhibition is the area appeared around pure and Na-doped ZnO samples coated in the disk at each respective concentrations where the growth of the microorganisms was arrested by the pure and Na-doped ZnO nanopowders. The measurement of the zone of inhibition was expressed in mm [27].

3. Results and discussion

3.1. XRD analysis

Fig. 2 shows the XRD patterns of as-synthesized pure and Na doped ZnO nanopowders. The XRD spectra of grown $Zn_{1-x}Na_xO$ samples show the various diffraction peaks corresponding to (100), (002), (101), (102), (110), (103), (200), (112), (201), (004) and (202) planes [28]. It is clear from XRD spectra line broadening; the co-precipitation synthesized powders are in nano-scale [6]. All the diffraction patterns of $Zn_{1-x}Na_xO$ confirmed the formation of hexagonal wurtzite structure of Zinc Oxide (JCPDS # 36-1451) [29]. No signal of extra diffraction peaks could be detected in this range of XRD corresponding to the sodium and its compounds due to its doping, leading to the formation of high purity single phase nanopowder samples. It is observed that Na ions are well doped into the hexagonal wurtzite ZnO matrix [30].

The average crystallite size (D) of Na doped ZnO nanostructures were calculated by using Debye-Scherrer's formula

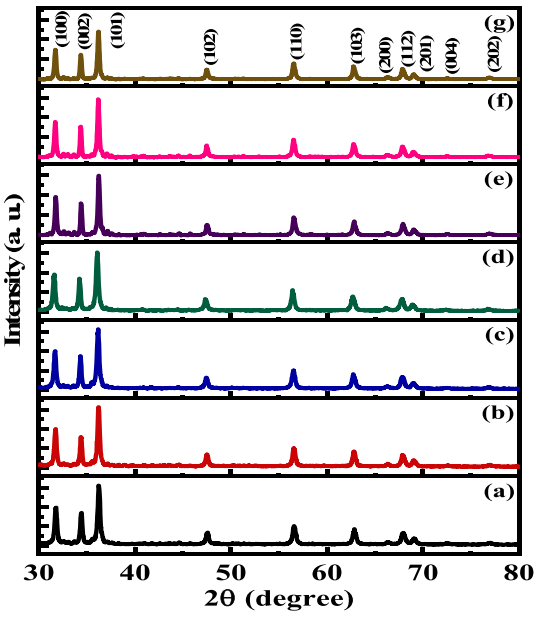

Fig. 2. X-ray diffraction pattern of $Zn_{1-x}Na_xO$ nanopowders, for × is equals to (a) 0, (b) 0.01, (c) 0.02, (d) 0.04, (e) 0.06, (f) 0.08 and (g) 0.10.

$$D(nm) = \frac{K\lambda}{\beta cos\theta} \quad (3)$$

where K is the constant with value 0.94, λ represents wavelength of the X-ray of CuKα radiation (0.154 nm), β is the full width at half maximum (FWHM) of the diffraction peak and θ is the Bragg's angle and **D** is the crystallite size in nm. From the line broadening of XRD (Fig. 3a), it clearly indicates that the mean crystallite size is increases from 23.51 to 28.11 nm with increasing Na doping concentration.

The dislocation density (δ) is defined as a measure of the amount of defects and vacancies in the crystal, which can be calculated from the average crystallite size (D) using the formula,

$$\delta = \frac{1}{D^2} \quad (4)$$

and the micro strain (ε) of the samples induced was determined by

$$\varepsilon = \frac{\beta cos\theta}{4} \quad (5)$$

respectively [31].

The calculated dislocation density and lattice strain both decreases with an increase in Na^+ ions doping concentration (Fig. 3b) due to the local distortion of lattice. The lattice cell volume (v) and bond length in Zn – O of $Zn_{1-x}Na_xO$ is increased up to $\times = 0.04$, then slightly decreases and is minimum for $\times = 0.06$ (Fig. 3a & c). The atom at $\times = 0.04$ could be trapped and shifted from the non-equilibrium to the more equilibrium position thereby releasing the lattice strain. Also, there was a slight shift in the diffraction peak positions of the $Zn_{1-x}Na_xO$ samples. These diffraction peak shifts change the lattice parameters a and c.

Table 1 shows how both the lattice parameters a and c change as a function of Na doping concentration. The lattice constants a and c were found to be 3.250 and 5.207 Å for pure ZnO; and 3.255 and 5.214 Å for $Zn_{0.90}Na_{0.10}O$ samples, respectively (Fig. 3d). This variation of the lattice constants (a and c) and the lattice cell volume (v) is due to the following two aspects: (i) the size variation of the ionic radii of Zn^{2+} (0.74 Å) and Na^+(1.02 Å) and (ii) Increase in free carriers causes deformation of the conduction band potential [32,33].

The comparison of structural parameters such as Bragg's angle (2θ), FWHM (β), crystallite size (D) and inter-planar distance (d) of $Zn_{1-x}Na_xO$ (x = 0.00–0.10) for (1 0 1) diffraction peak were provided in Table 2 and it is observed that the inter planar spacing (d) was slightly varying with increasing Na concentration.

The bond length L (Å) of Zn – O is given by [34]:

$$L = \left[\left(\frac{a^2}{3}\right) + \left(\frac{1}{2} - u\right)^2 c^2\right]^{1/2} \quad (6)$$

Where a and b are lattice parameters and u denote the positional parameter, which measures the amount of displacement of each atom w. r.t. next atom along the c – axis in the wurtzite hexagonal structure and is given by:

$$u = \frac{a^2}{3c^2} + 0.25 \quad (7)$$

The reported bond length L (Å) value of Zn – O in the undoped ZnO unit cell viewed in a direction parallel to Zn^{2+} and O^{2-} atoms was given 1.9767 Å [35]. It can be observed that the calculated L(Å) values of as-prepared nanopowders matches well with the reported value and its variation with Na doping concentration is shown in Fig. 3a.

The Williamson and Hall graphs (W – H graphs) are plotted between 4 sinθ on X – axis and β_{hkl} cosθ on Y – axis for preferred peaks of diffraction of $Zn_{1-x}Na_xO$ nanoparticles are shown in Fig. 4. In W-H methodology, the average crystallite size (D_{avg}) and the micro strain (ε) of the pure and Na-doped ZnO samples are calculated from the y-intercept and slope of linear plot [36]. The structural parameters D_{avg} and ε values evaluated from W – H method are 40.78 nm and 0.00139 for pure ZnO; and 34.75 nm and 0.000825 for $Zn_{0.96}Na_{0.04}O$ samples,

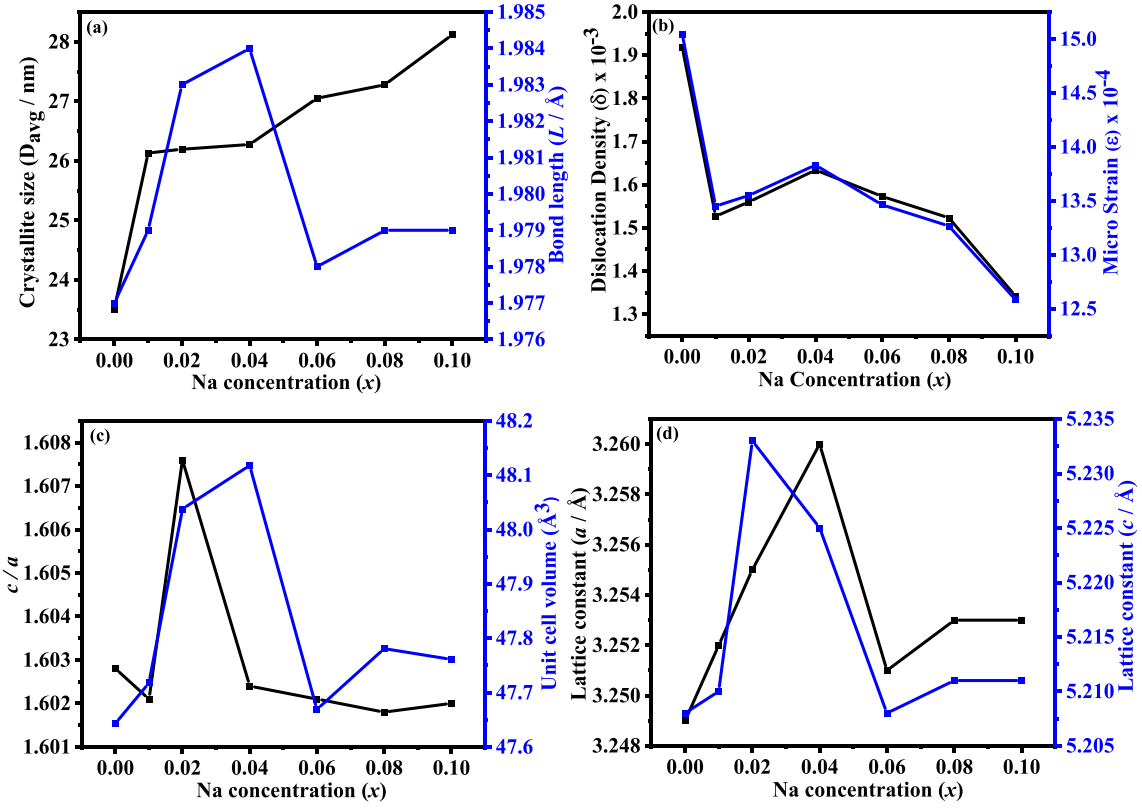

Fig. 3. The calculated structural parameters variations of $Zn_{1-x}Na_xO$ nanopowders with Na doping concentration **(a)** Average crystallite size and Bond length; **(b)** Dislocation density and Micro strain; **(c)** c/a ratio and Unit cell volume; and (d) Lattice constants (a and c).

Table 1
The average crystallite size, lattice constants (*a* and *c*) and unit cell volume of the $Zn_{1-x}Na_xO$ (x = 0–0.10) nano powders.

Na doping concentration (*x*)	Average crystallite size D_{avg} (nm)	Lattice Parameters *a* = *b* (Å)	*c* (Å)	*c* / *a* ratio	Average Unit cell volume (Å^3)	Dislocation density (δ)	Micro strain (ε)	Bond Length L (Å) of Zn-O
$x = 0$	23.510	3.249	5.208	1.6028	47.643	1.919E-03	15.046E-04	1.977
$x = 0.01$	26.131	3.252	5.210	1.6021	47.718	1.527E-03	13.452E-04	1.979
$x = 0.02$	26.196	3.255	5.233	1.6076	48.038	1.560E-03	13.549E-04	1.983
$x = 0.04$	26.275	3.260	5.225	1.6024	48.118	1.634E-03	13.833E-04	1.984
$x = 0.06$	27.051	3.251	5.208	1.6021	47.669	1.573E-03	13.463E-04	1.978
$x = 0.08$	27.280	3.253	5.211	1.6018	47.781	1.523E-03	13.267E-04	1.979
$x = 0.10$	28.119	3.253	5.211	1.6020	47.761	1.342E-03	12.583E-04	1.979

Table 2
The Bragg's angle (2θ), FWHM (β), crystallite size (D) and inter-planar distance (d) of $Zn_{1-x}Na_xO$ (x = 0–0.10) for (1 0 1) diffraction peak.

Na doping Concentration (*x*)	Bragg's angle (2θ) (Deg)	FWHM β (Deg)	D (nm)	Inter planar distance (d) (Å)
$x = 0$	36.251	0.323	25.807	2.476
$x = 0.01$	36.218	0.301	27.694	2.478
$x = 0.02$	36.163	0.303	27.535	2.481
$x = 0.04$	36.075	0.275	30.348	2.487
$x = 0.06$	36.242	0.247	33.732	2.476
$x = 0.08$	36.192	0.251	33.271	2.479
$x = 0.10$	36.203	0.260	32.133	2.479

respectively.

3.2. The UV–Vis optical absorption spectra

UV–Visible absorption spectra are formed by suspending the as-prepared samples in deionized water for a long period of time at room temperature. Various optical absorption peaks were observed due to large exciton binding energy (60 mV) [6]. The UV–Vis optical absorption pattern of $Zn_{1-x}Na_xO$ nanopowders in the wavelength the range of 200 – 800 nm are showed in Fig. 5. The absorption peaks of $Zn_{0.99}Na_{0.01}O$ samples were recorded at 196, 284 and 365 nm, respectively and it is evident that all Na-doped ZnO samples shows excellent optical absorbance below the wavelength of 390 nm while a very small absorbance was found in the visible region. From the spectra it is obvious that Na doped ZnO strongly absorb around 370 nm compared to pure ZnO due to presence of sodium content [8]. These absorption peaks are due to the electronic transitions from deep level of valence band to conduction band. Due to the difference in the particle size and shape of $Zn_{1-x}Na_xO$ samples, the UV–Vis absorption peak pattern was slightly varying with an increase in Na^+ doping content [28].

The optical direct band gap of $Zn_{1-x}Na_xO$ samples is determined by Tauc's formula,

$$(\alpha h\upsilon)^n = B\left(h\upsilon - -E_g\right) \quad (7)$$

where, **B** is a constant of the material, **hν** is the incident photon energy in eV, **h** is Planck's constant, $\mathbf{E_g}$ is the optical energy bandgap in eV, **n** is an exponent and n = 2/3, 1/3, 2 and 1/2 for direct forbidden, indirect forbidden, direct allowed and indirect allowed transitions respectively, and **α** is the absorption coefficient (in cm^{-1}) [31].

Plots of $(\alpha h\upsilon)^2$ vs photon energy (hν) of pure and Na doped ZnO samples are illustrated in Fig. 6. The direct allowed band gap energy (E_g) for which n = 2 is measured by the extrapolation of the linear portions of the curves on the X-axis as shown in the Fig. 6. Bulk form of ZnO has a direct gap of 3.15 eV. It can be noticed that the band gap measured in nano sized form is higher than the value of bulk ZnO as in the nano scale,

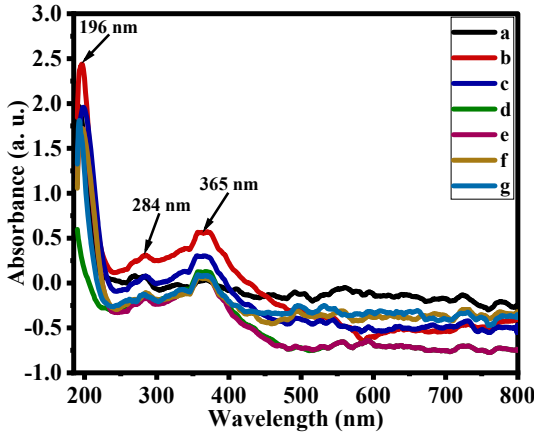

Fig. 5. Optical absorption spectra of $Zn_{1-x}Na_xO$ samples; (a) × = 0, (b) × = 0.01, (c) × = 0.02, (d) × = 0.04, (e) × = 0.06, (f) × = 0.08 and (g) × = 0.10.

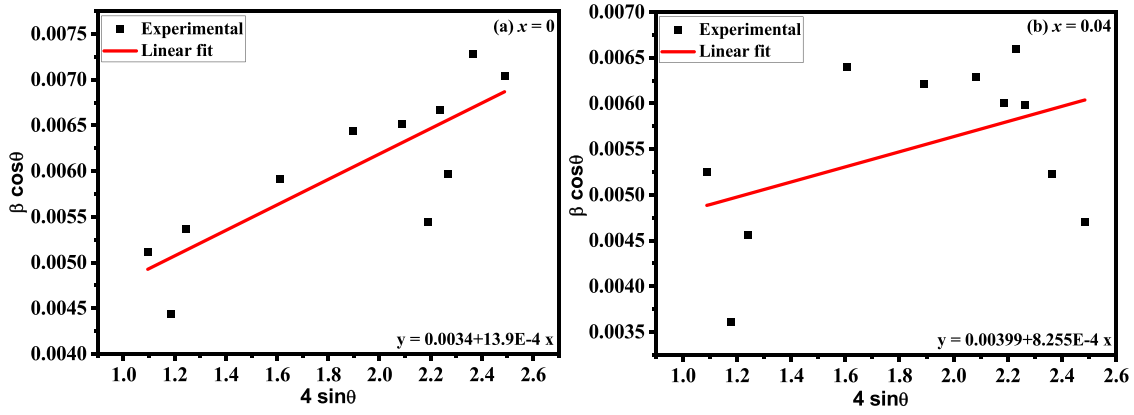

Fig. 4. W-H plots of $Zn_{1-x}Na_xO$ nanopowders; (a) × = 0 and (b) × = 0.04.

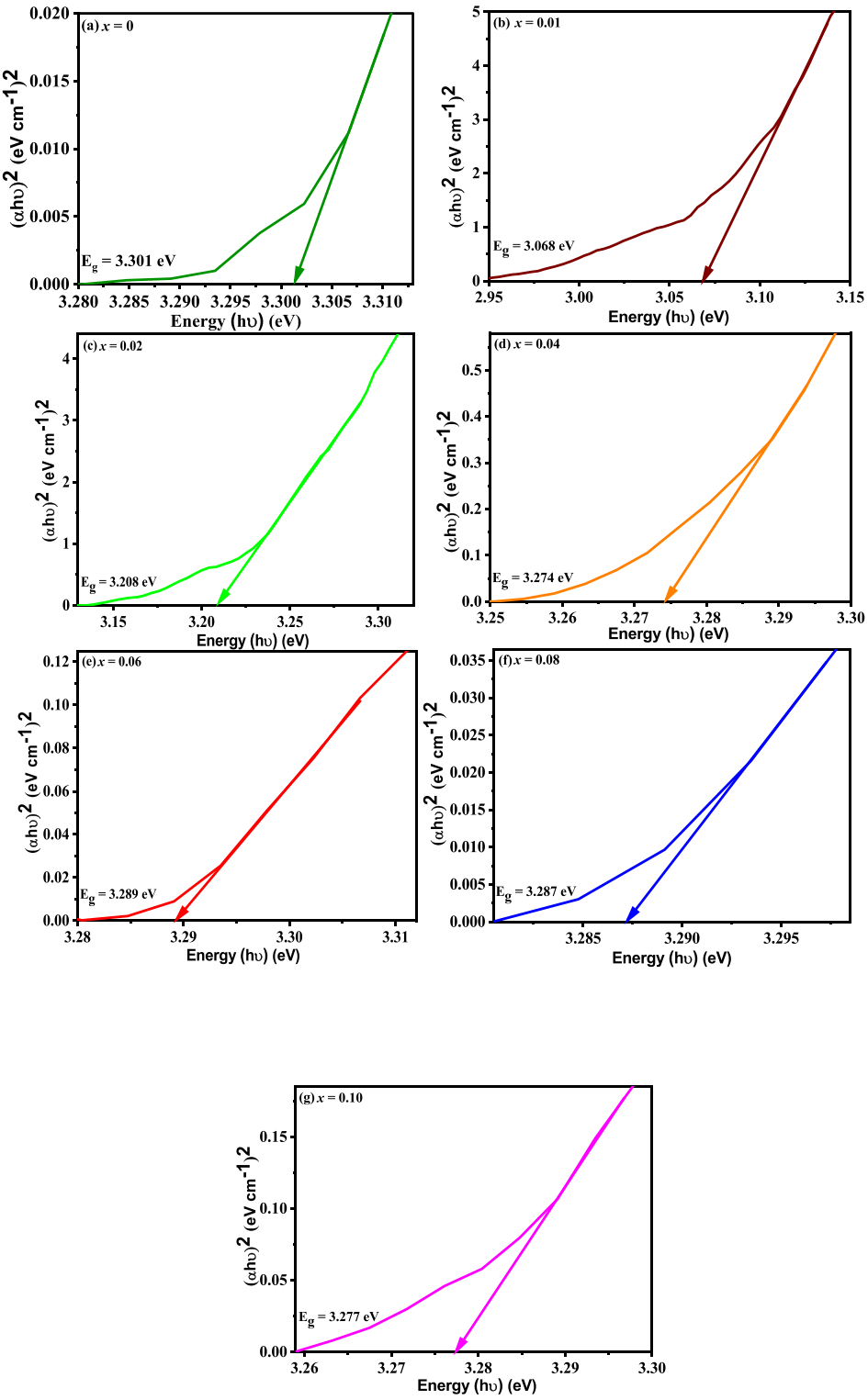

Fig. 6. Tauc plot of $[\alpha h\nu]^2$ versus photon energy ($h\nu$) to determine the band gap E_g of the as-prepared $Zn_{1-x}Na_xO$ nanopowders; (a) × = 0, (b) × = 0.01, (c) × = 0.02, (d) × = 0.04, (e) × = 0.06, (f) × = 0.08 and (g) × = 0.10.

the electronic levels become completely discrete in atoms and molecules of a semiconductor [37 –40].

Furthermore, the band gap energy (E_g) of the Na doped ZnO nanopowders increases up to × = 0.06 and reached maximum (3.289 eV), then slowdown and decreases as Na doping concentration increases as depicted in Fig. 7. This significant behaviour of E_g is due to the modification of electronic structural of ZnO over Na sustitution. So, it is clear that the synthesized $Zn_{1-x}Na_xO$ samples show the quantum-confinement effect.

3.3. FTIR studies

Fig. 8 represents the FTIR spectroscopic pattern of $Zn_{1-x}Na_xO$ nanopowders, which showed various peaks at 3412, 2996, 2360, 1550, 1391,

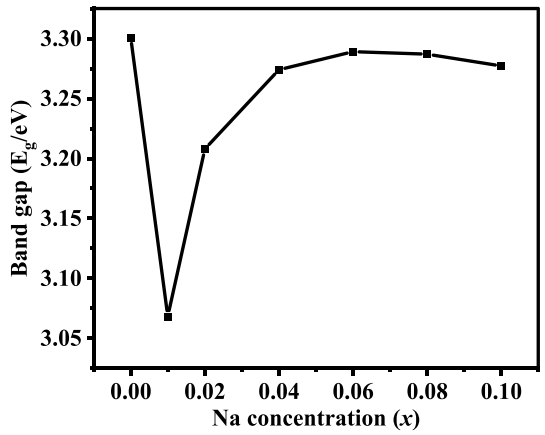

Fig. 7. The calculated variation of energy band gap (E_g) of wurtzite $Zn_{1-x}Na_xO$ nanopowders as a function of the Na doping concentration (*x*).

1018, 796, 633 and 425 cm^{-1} for $Zn_{0.90}Na_{0.10}O$ sample. The important functional groups such as ZnO, carboxylate (COO–) and hydroxyl (O–H) impurities can be seen. From the figure, the absorption band at 425 cm^{-1} is attributed to the Zn–O stretching vibration mode of phonons of the samples. The peaks around 633 cm^{-1} attributed to the existence of Na in Zinc Oxide lattice [10]. The O–H stretching mode of vibration found around 3412 cm^{-1}, which is a confirmation of presence of hydroxyl groups and water molecule on the surface of ZnO nanoparticles. The small absorption peaks about 2360 and 2996 cm^{-1} corresponds to C–H stretching vibration of alkane groups. C–O stretching modes of vibration corresponds to 1018 cm^{-1} and the symmetric and asymmetric stretching mode of vibration bands due to C=O and carboxylate found at 1550 and 1391 cm^{-1}, which is attributed to the Zinc Oxide nanopowders during co-precipitation synthesis [41]. This functional group appeared due to the non-uniform decomposition of the acetate group with mixed precursor solution. The FTIR analysis indicates the successful formation of hexagonal wurtzite ZnO nanoparticles. Table 3 provided information about the peak positions, nature of the peak, and vibrational modes from FTIR spectroscopic data of molecules of $Zn_{0.90}Na_{0.10}O$. From the Fig. 8, the FT-IR data of synthesized Na doped ZnO samples are similar to that of the pure ZnO. The modes of vibrations are slightly changes due to mismatch between ionic radius of Na^+ and Zn^{2+} which attributes the activation of defects and oxygen vacancies in the intrinsic host lattice of ZnO. So the red shift in the vibrational modes was caused by these activated impurities [42].

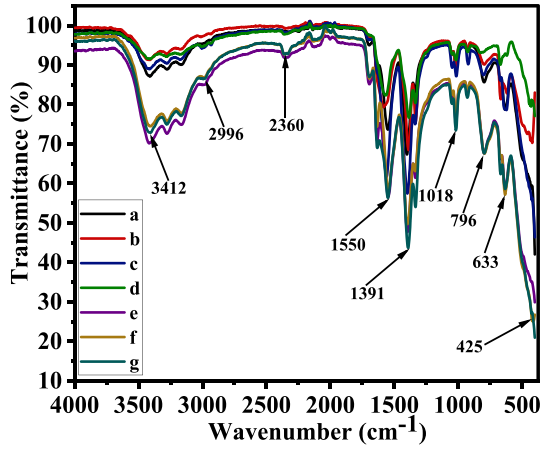

Fig. 8. FTIR spectra of $Zn_{1-x}Na_xO$ nanopowders; (a) × = 0, (b) × = 0.01, (c) × = 0.02, (d) × = 0.04, (e) × = 0.06, (f) × = 0.08 and (g) × = 0.10.

Table 3
FTIR spectroscopic data including absorption peaks and the corresponding functional groups of $Zn_{0.90}Na_{0.10}O$ sample.

S. No.	Absorption peak position (cm^{-1})	Nature	Bond/ Functional groups
1	3412	Very strong	–OH stretching mode
2	2996	Weak	C–H stretching mode of alkane groups
3	2360	Weak	C–H stretching vibration mode
4	1550	Very strong	ν_s (C–O) + δ (OC = O)
5			
6	1391	Very Strong	ν_s (C–O) + δ (OC = O)
7	1018	Strong	ν_s (C–O)
8	796	Weak	C–C stretching
9	633	Weak	Existence of Na in ZnO lattice
10	425	Strong	ZnO stretching vibration

3.4. Scanning Electron microscopy (SEM) analysis

Scanning Electron Microscopy (SEM) technique was used to examine the size, shape of the nanoparticles and surface morphology which includes topographical, morphological structures and growth mechanism of the particles. Fig. 9**(a–d)** shows the SEM micrographs of undoped and Na doped ZnO samples. These images clearly indicate the formation of nanoparticles with average size in the order of nanometer scale exhibiting hexagonal structure, which is also confirmed by XRD analysis. The morphology of $Zn_{1-x}Na_xO$ nanopowders contain mixer of uniformly distributed rod-like and bar-like particles in its morphology [43]. The particle size increases with increasing Na doping concentration. As sodium content increases, the shape of the particle's is changing from rod-like to non-uniform shaped stone-like structures which showed the structural morphology largely depends on the doping concentration. In all cases, an agglomeration of nanoparticles was observed due to densification of dispersed particles. Particularly, $Zn_{1-x}Na_xO$ samples consist of small number of stone-like and large number of rod / bar-like structures with the average diameters of around 375 nm and 273.5 nm, respectively. The crystallite sizes evaluated from the powder XRD calculations do not match well with the particle grain sizes obtained from SEM micrographs as the grains formed in the SEM images are the domains consists of aggregation of the nano-size crystallites (in the XRD) [11]. It can be seen that the powder XRD technique is more stringent method which leads to smaller sizes [44]. So, the substitution of Na influences changes in the shape, the crystallization and growth of ZnO nanoparticles and also causes an increase in the size of nanoparticles for higher concentration [45].

3.5. EDX spectroscopy

The Energy Dispersive X-ray (EDX) data gives the information about the elemental composition in atomic and weight percentage terms of the pure and Na doped ZnO nanopowders. The EDX analysis of $Zn_{1-x}Na_xO$ samples were shown in Fig. 10**(a-b)**. From the EDX images, it clearly indicates that the intensity and amount of Na element in the as-synthesized samples increases with increasing Na doping concentration. The peaks present in the EDX pattern may be related to Zn, Na and O only [30,41]. It can be evident that no other dispersive peaks were observed related to foreign elements and impurities, which provides the confirmation about the formation of single-phase sodium doped ZnO nanopowders [46]. Also, there are no independent peaks resulting from sodium and its compounds in the $Zn_{1-x}Na_xO$samples indicating the complete dissolution of sodium into ZnO crystal lattice.

EDX elemental analysis histogram depicts the number of different elements of $Zn_{1-x}Na_xO$ nanopowders in weight percentage, as shown in

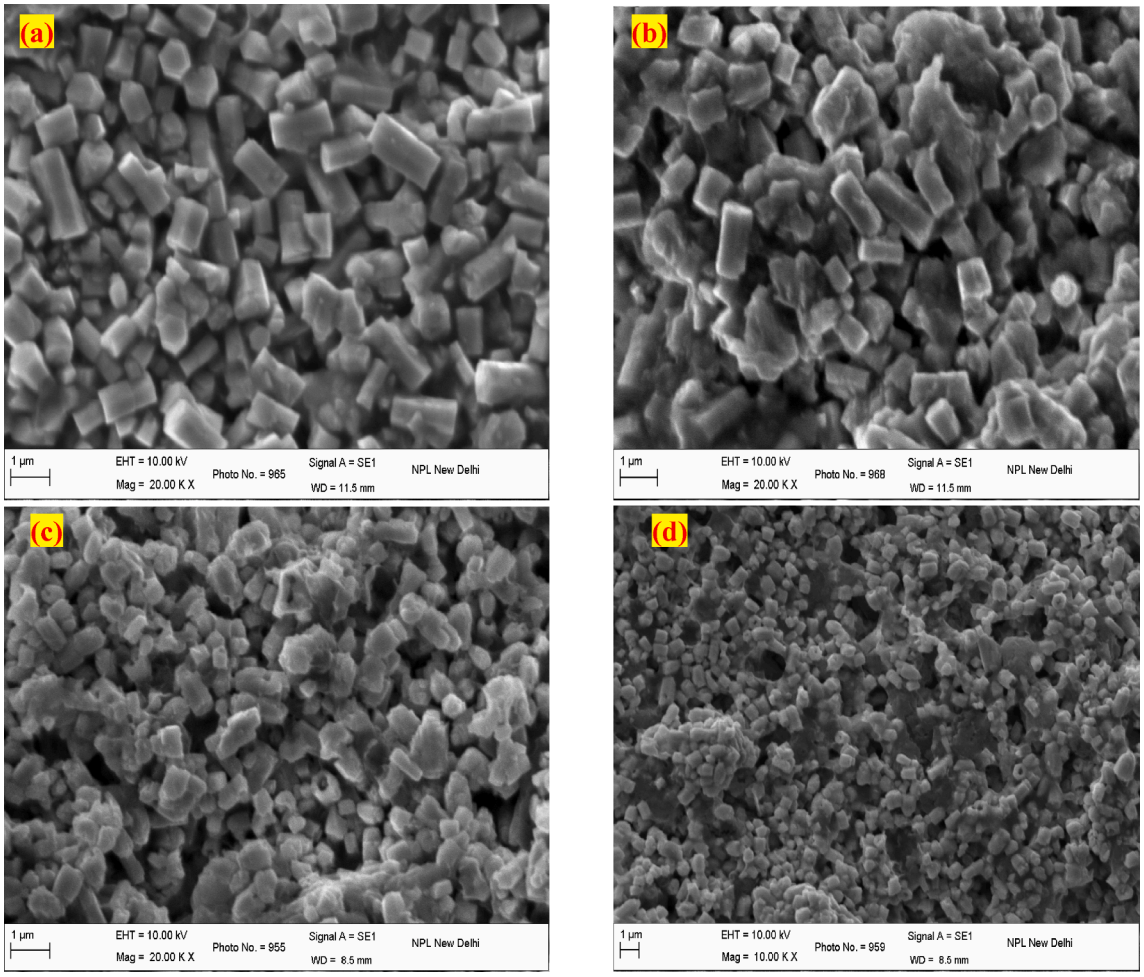

Fig. 9. (a - d) SEM micrographs of $Zn_{1-x}Na_xO$ nanopowders; (a) × = 0, (b) × = 0.02, (b) × = 0.06, and (d) × = 0.10.

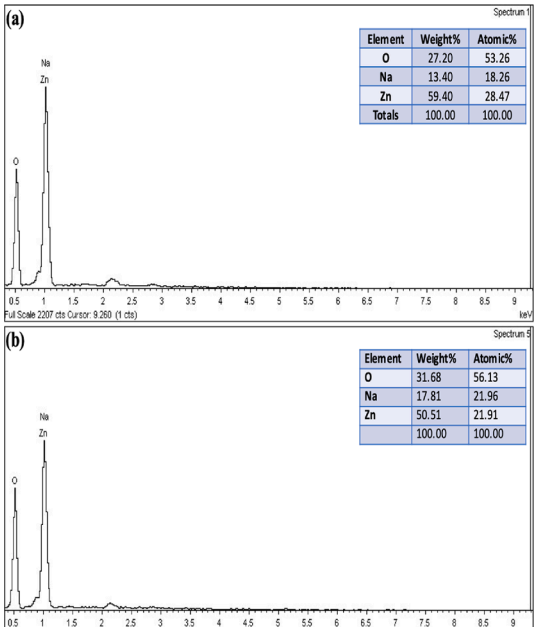

Fig. 10. EDX analysis of (a) $Zn_{0.99}Na_{0.01}O$ and (b) $Zn_{0.90}Na_{0.10}O$ samples.

the Fig. 11. Clearly, the measured amounts of Zn and O elements are higher than that of the Na element in the as-synthesized samples.

3.6. Antibacterial and antifungal activity

The antibacterial activity of pure and graded concentrations of Na doped ZnO samples was tested using disk diffusion method against selected four different bacterial cultures namely *Escherichia coli,*

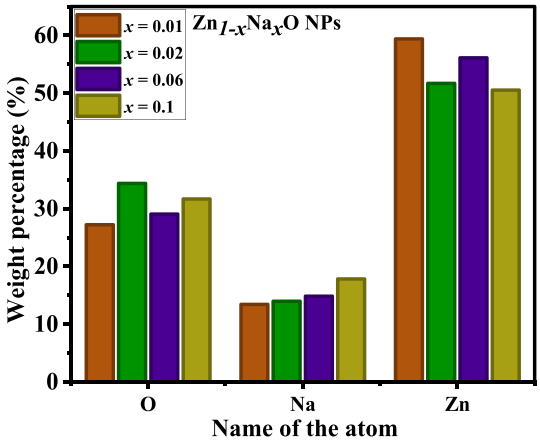

Fig. 11. Elemental analysis histogram representation in weight percentage of selected $Zn_{1-x}Na_xO$ samples.

Pseudomonas aeruginosa, *Klebsiella neumoniae* and *Staphylococcus aureus*. The Inhibition zone around the graded sample in the disc was depicted in the Fig. 12 and the estimated values of Zone of Inhibition in mm are plotted as histogram (Fig. 13) [46]. The results showed that the pure and Na doped ZnO nanopowders exhibit excellent bacterial growth in the disc for all bacteria; *E. coli, P.* aeruginosa, *K. neumoniae* and *S. aureus*. It is noted that the dose dependent highest growth inhibitory zone was observed with the increased dopant concentrations of Na than pure ZnO and the superior zone of Inhibition was obtained for $Zn_{0.90}Na_{0.10}O$ samples for all the bacterial strains.

The Antifungal activity of pure and Na doped ZnO nanopowders was also studied with different Na concentrations against two fungi *Candida* and *Aspergillus,* respectively. In the case of Candida as shown in Fig. 14(a - b), the Inhibition zone is found to increase proportionally with increasing Na doping concentration and the highest Inhibition was observed at higher concentrations. No Inhibitory zone is obtained for control which is prepared using the stack without zinc oxide and tested in the disc. However, in the case of *Aspergillus* as depicted Fig. 14(c - d), the Zone of Inhibition is observed same at lower Na doping concentrations and obtained enhanced zone at higher concentrations. It can also be noted that, the increased Na dopant have shown more growth inhibitory effect against the fungal pathogens *Candida* and *Aspergillus* when compared to pure ZnO nanoparticles, which was evident in Fig. 15 [47]. The present study reported a significant high growth inhibitory zone against pure ZnO [48,49]. The results were noticed as extremely significant and the values are Mean ± SD (n = 4). *P < 0.0001 Compared to control (Pure ZnO).

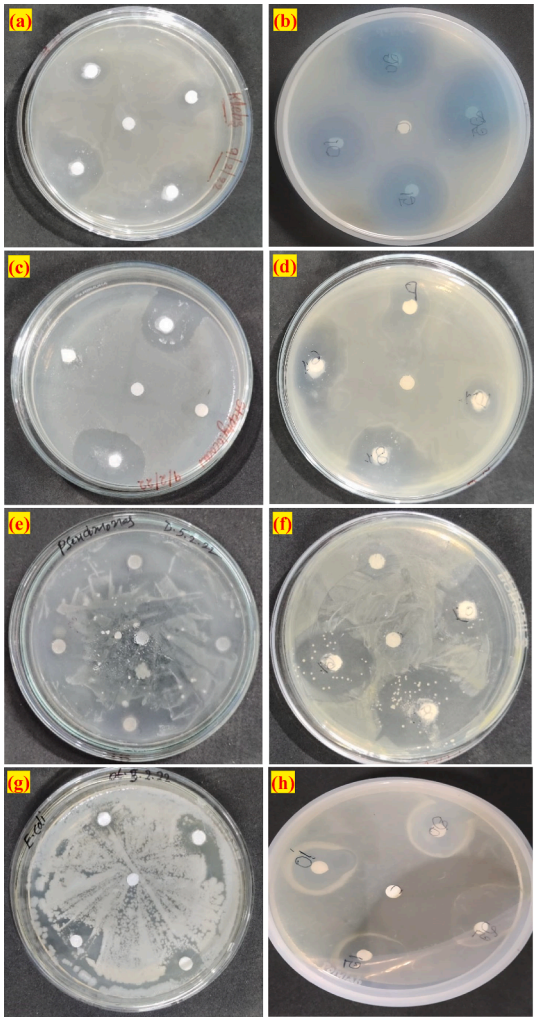

Fig. 12. Antibacterial activity of pure and Na doped ZnO nanoparticles against standard human pathogenic bacteria (**a-b:** *Klebsiella pneumoniae;* **c-d:** *Staphylococcus aureus;* **e-f:** *Pseudomonas aeruginosa*; and **g-h:** *Escherichia coli)*.

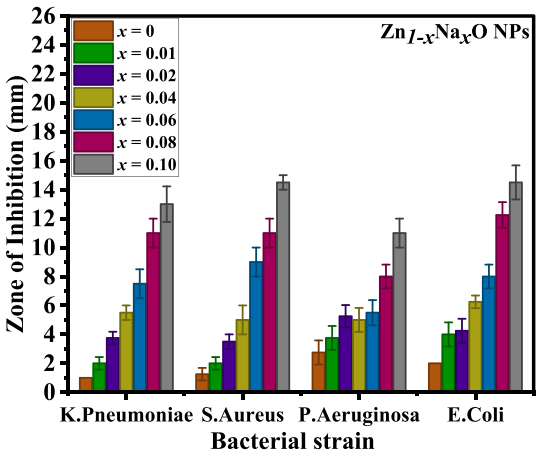

Fig. 13. The Zone of inhibition of pure and Na doped ZnO nanoparticles against Bacterial cultures. The values are Mean ± SD (n = 4). *P < 0.0001 Compared to control (Pure ZnO).

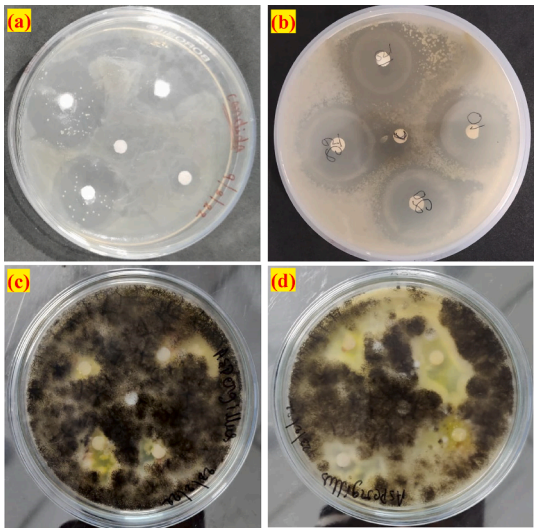

Fig. 14. Potent antifungal activity of pure and Na doped ZnO nanoparticles against pathogenic fungi (**a-b:** *Candida;* and **c-d:** *Aspergillus)*.

4. Conclusions

In the present work, $Zn_{1-x}Na_xO$ nanopowders have been successfully synthesized by a simple co-precipitation method. It was evident from XRD studies that the as-synthesized $Zn_{1-x}Na_xO$ nanopowders exhibits hexagonal wurtzite structure and the average crystallite size determined by using the Scherrer formula increases and the calculated bond length L (Å) values were slightly varies with increase in Na-doping concentration. The average diameter estimated by the SEM micrographs of the prepared samples also increases, which confirms the surface area reduction with Na content. The FTIR analysis shows the presence of precursors and the formation of functional ZnO and Na doped ZnO nanopowders. The results obtained from UV – Vis spectroscopic data shows the suffered band gap between 3.068 and 3.301 eV and affected optical absorption band with the presence of Na concentration. The energy dispersive X-ray study confirms the successful incorporation of Na in the ZnO lattice. Antibacterial study against the microorganisms E. coli, P. aeruginosa, K. pneumoniae and *S. aureus* reveals that the zone of

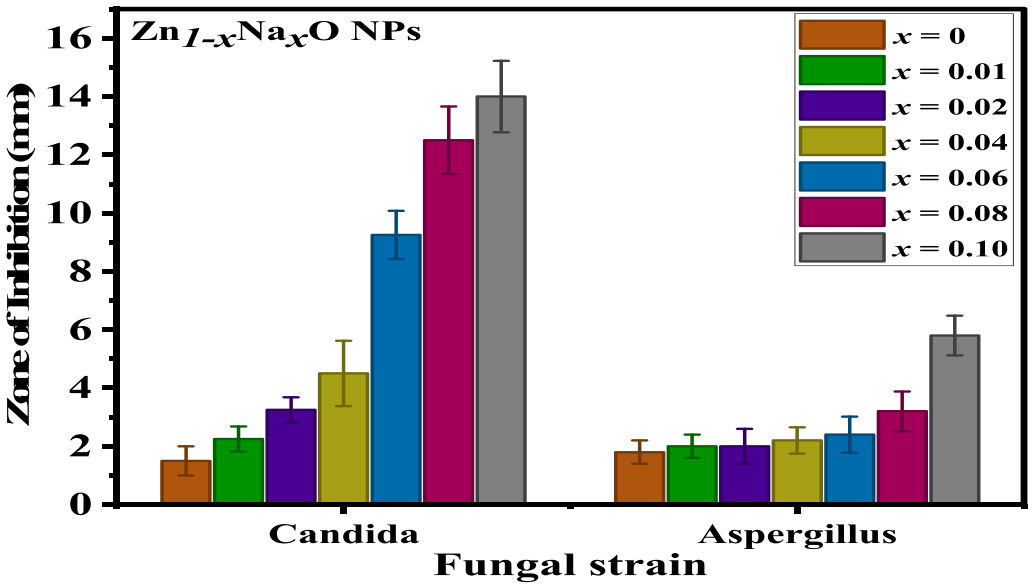

Fig. 15. The Zone of inhibition of pure and Na doped ZnO nanoparticles against fungal cultures. The values are Mean ± SD (n = 4). *P < 0.0001 Compared to control (Pure ZnO).

inhibition increases with increase in Na doping content. The antifungal study against the fungal pathogens *Aspergillus* and *Candida* shows that in case of *Candida* the inhibition zone increases with increase in Na concentration but in case of *Aspergillus* the inhibition zone is remained same for all Na concentrations except at very high concentrations. This study concluded that the as-synthesized nano powders may be used as antibacterial agents and antifungal medication in pharmaceutical applications.

CRediT authorship contribution statement

B. Nageswara Rao: Writing – original draft. **P. Tirupathi Rao:** Visualization, Investigation. **K. Vasudha:** Visualization, Investigation. **Sk. Esub Basha:** Writing – original draft. **D.S.L. Prasanna:** Writing – original draft. **T. Bhushana Rao:** Writing – original draft. **K. Samatha:** Writing – review & editing. **R.K. Ramachandra:** Conceptualization, Methodology, Supervision.

Declaration of Competing Interest

The authors declare that they have no known competing financial interests or personal relationships that could have appeared to influence the work reported in this paper.

Data availability

Data will be made available on request.

Acknowledgements

The authors are thankful to DST-FIST – Central Instrumentation Laboratory & Department of Physics, Government College (Autonomous), Rajahmundry, Andhra Pradesh and National Physical Laboratory (CSIR-NPL), New Delhi

References

[1] A. Naveed Ul Haq, A. Nadhman, I. Ullah, G. Mustafa, M. Yasinzai, I. Khan, Synthesis Approaches of Zinc Oxide Nanoparticles: The Dilemma of Ecotoxicity, Journal of Nanomaterials. 2017 (2017) 1–14.
[2] S. Sabir, M. Arshad, S.K. Chaudhari, Zinc Oxide Nanoparticles for Revolutionizing Agriculture: Synthesis and Applications, The Scientific World Journal. 2014 (2014) 1–8, https://doi.org/10.1155/2014/925494.
[3] A. Janotti, C.G. Van de Walle, Fundamentals of zinc oxide as a semiconductor, Rep. Prog. Phys. 72 (12) (2009) 126501.
[4] V. Parihar, M. Raja, R. Paulose, A Brief Review of Structural, Electrical and Electrochemical Properties of Zinc Oxide Nanoparticles, REVIEWS ON ADVANCED MATERIALS SCIENCE. 53 (2018) 119–130, https://doi.org/10.1515/rams-2018-0009.
[5] M. Snure, A. Tiwari, Band-gap engineering of $Zn_{1-x}Ga_xO$ nanopowders: Synthesis, structural and optical characterizations, J. Appl. Phys. 104 (2008), 073707, https://doi.org/10.1063/1.2988131.
[6] A. Vanaja, G.V. Ramaraju, S. Rao, Structural and Optical Investigation of Al Doped ZnO Nanoparticles Synthesized by Sol-gel Process, Indian Journal of Science and Technology. 9 (2016). https://doi.org/10.17485/ijst/2016/v9i12/87013.
[7] M. Chitra, K. Uthayarani, N. Rajasekaran, E.K. Girija, Preparation and Characterisation of Al doped ZnO Nanopowders, Physics Procedia. 49 (2013) 177–182, https://doi.org/10.1016/j.phpro.2013.10.024.
[8] S. Al-Ariki, N.A.A. Yahya, S.A. Al-A'nsi, M.H.H. Jumali, A.N. Jannah, R. Abd-Shukor, Synthesis and comparative study on the structural and optical properties of ZnO doped with Ni and Ag nanopowders fabricated by sol gel technique, Sci Rep. 11 (1) (2021), https://doi.org/10.1038/s41598-021-91439-1.
[9] J. El Ghoul, M. Kraini, L. El Mir, Synthesis of Co-doped ZnO nanoparticles by sol–gel method and its characterization, J Mater Sci: Mater Electron. 26 (2015) 2555–2562, https://doi.org/10.1007/s10854-015-2722-z.
[10] B. Babu, V.P. Manjari, T. Aswani, G.T. Rao, R.J. Stella, R.V.S.S.N. Ravikumar, Structural, optical and magnetic properties of Cr^{3+} doped ZnO nanopowder, Indian, J Phys. 88 (2014) 683–690, https://doi.org/10.1007/s12648-014-0473-y.
[11] U.S. Udayachandran Thampy, C.h. Rama Krishna, C.h. Venkata Reddy, B. Babu, Y. P. Reddy, P.S. Rao, R.V.S.S.N. Ravikumar, Spectral Investigations on Cu^{2+}-Doped ZnO Nanopowders, Appl Magn Reson. 41 (2011) 69–78, https://doi.org/10.1007/s00723-011-0234-4.
[12] L. Armelao, G. Bottaro, M. Pascolini, M. Sessolo, E. Tondello, M. Bettinelli, A. Speghini, Structure−Luminescence Correlations in Europium-Doped Sol−Gel ZnO Nanopowders, J. Phys. Chem. C. 112 (2008) 4049–4054, https://doi.org/10.1021/jp710207r.
[13] M.A. Ciciliati, M.F. Silva, D.M. Fernandes, M.A.C. de Melo, A.A.W. Hechenleitner, E.A.G. Pineda, Fe-doped ZnO nanoparticles: Synthesis by a modified sol–gel method and characterization, Materials Letters. 159 (2015) 84–86, https://doi.org/10.1016/j.matlet.2015.06.023.
[14] H. Shokry Hassan, A.B. Kashyout, I. Morsi, A.A.A. Nasser, I. Ali, Synthesis, characterization and fabrication of gas sensor devices using ZnO and ZnO: In nanomaterials, Beni-Suef University Journal of Basic and Applied Sciences. 3 (2014) 216–221, https://doi.org/10.1016/j.bjbas.2014.10.007.
[15] L. Fadillah, B. Soegijono, S. Budiawanti, I. Mudzakir, Fabrication and characterization of ZnO and Li doped ZnO by a sol-gel method, in: Depok, Jawa Barat, Indonesia, 2017: p. 030053. https://doi.org/10.1063/1.4991157.
[16] P.D. Candra Seta, P.E. Yunita, M.A. Baqiya, Darminto, Structural and Magnetic Characterization of Mn and Fe–doped ZnO Nanopowders, IOP Conf. Ser.: Mater. Sci. Eng. 196 (2017), 012018, https://doi.org/10.1088/1757-899X/196/1/012018.
[17] A. Sayari, L.E. Mir, Structural and Optical Characterization of Ni and Al Co-Doped ZnO Nanopowders Synthesized via the Sol-Gel Process, KONA. 32 (2015) 154–162. https://doi.org/10.14356/kona.2015003.

[18] N.S. Parmar, K.G. Lynn, Sodium doping in ZnO crystals, Appl. Phys. Lett. 106 (2) (2015) 022101.
[19] S. Fabbiyola, L.J. Kennedy, U. Aruldoss, M. Bououdina, A.A. Dakhel, J. JudithVijaya, Synthesis of Co-doped ZnO nanoparticles via co-precipitation: Structural, optical and magnetic properties, Powder Technology. 286 (2015) 757–765, https://doi.org/10.1016/j.powtec.2015.08.054.
[20] P.G. Devi, A.S. Velu, Synthesis, structural and optical properties of pure ZnO and Co doped ZnO nanoparticles prepared by the co-precipitation method, J Theor Appl Phys. 10 (2016) 233–240, https://doi.org/10.1007/s40094-016-0221-0.
[21] T.T. Ha, T.D. Canh, N.V. Tuyen, A Quick Process for Synthesis of ZnO Nanoparticles with the Aid of Microwave Irradiation, ISRN Nanotechnology. 2013 (2013) 1–7, https://doi.org/10.1155/2013/497873.
[22] L. Chandra, P.K. Sahu, R. Dwivedi, V.N. Mishra, Synthesis of Na doped ZnO nanoparticles for detection of reducing gases, in: in: 2016 IEEE Uttar Pradesh Section International Conference on Electrical, Computer and Electronics Engineering (UPCON), IEEE, Varanasi, India, 2016, pp. 102–105, https://doi.org/10.1109/UPCON.2016.7894633.
[23] S.V. Gudkov, D.E. Burmistrov, D.A. Serov, M.B. Rebezov, A.A. Semenova, A. B. Lisitsyn, A Mini Review of Antibacterial Properties of ZnO Nanoparticles, Front. Phys. 9 (2021), 641481, https://doi.org/10.3389/fphy.2021.641481.
[24] A.W. Bauer, W.M. Kirby, J.C. Sherris, M. Turck, Antibiotic susceptibility testing by a standardized single disk method, Am J Clin Pathol. 45 (1966) 493–496.
[25] A.T. Ravichandran, R. Karthick, K. Ravichandran, D. Ravinder, R. Chandramohan, Revealing the influence of the Bi dopant on the structural, photoluminescence and antibacterial properties of ZnO nanoparticles, J Mater Sci: Mater Electron. 29 (2018) 2784–2790, https://doi.org/10.1007/s10854-017-8206-6.
[26] N. Mahmoudi Khatir, Z. Abdul-Malek, A.K. Zak, A. Akbari, F. Sabbagh, Sol–gel grown Fe-doped ZnO nanoparticles: antibacterial and structural behaviors, J Sol-Gel Sci Technol. 78 (2016) 91–98, https://doi.org/10.1007/s10971-015-3922-y.
[27] B.-L. Guo, P. Han, L.-C. Guo, Y.-Q. Cao, A.-D. Li, J.-Z. Kong, H.-F. Zhai, D. Wu, The Antibacterial Activity of Ta-doped ZnO Nanoparticles, Nanoscale Res Lett. 10 (2015) 336, https://doi.org/10.1186/s11671-015-1047-4.
[28] G. S, A. Belay, C. Reddy AR, B. Z, Synthesis and Characterizations of Zinc Oxide Nanoparticles for Antibacterial Applications, J Nanomed Nanotechnol. s8 (2017), https://doi.org/10.4172/2157-7439.S8-004.
[29] A. George, S.K. Sharma, S. Chawla, M.M. Malik, M.S. Qureshi, Detailed of X-ray diffraction and photoluminescence studies of Ce doped ZnO nanocrystals, Journal of Alloys and Compounds. 509 (2011) 5942–5946, https://doi.org/10.1016/j.jallcom.2011.03.017.
[30] K. Pradeev raj, K. Sadaiyandi, A. Kennedy, S. Sagadevan, Z.Z. Chowdhury, M.R. B. Johan, F.A. Aziz, R.F. Rafique, R. Thamiz Selvi, R. Rathina bala, Influence of Mg Doping on ZnO Nanoparticles for Enhanced Photocatalytic Evaluation and Antibacterial Analysis, Nanoscale Res Lett. 13 (1) (2018), https://doi.org/10.1186/s11671-018-2643-x.
[31] D. Saravanakkumar, S. Sivaranjani, K. Kaviyarasu, A. Ayeshamariam, B. Ravikumar, S. Pandiarajan, C. Veeralakshmi, M. Jayachandran, M. Maaza, Synthesis and characterization of ZnO–CuO nanocomposites powder by modified perfume spray pyrolysis method and its antimicrobial investigation, J. Semicond. 39 (3) (2018) 033001.
[32] M. Leszczynski, J. Bak-Misiuk, J. Domagala, J. Muszalski, M. Kaniewska, J. Marczewski, Lattice dilation by free electrons in heavily doped GaAs:Si, Appl. Phys. Lett. 67 (1995) 539–541, https://doi.org/10.1063/1.115181.
[33] M. Leszczynski, H. Teisseyre, T. Suski, I. Grzegory, M. Bockowski, J. Jun, S. Porowski, K. Pakula, J.M. Baranowski, C.T. Foxon, T.S. Cheng, Lattice parameters of gallium nitride, Appl. Phys. Lett. 69 (1996) 73–75, https://doi.org/10.1063/1.118123.
[34] R.K. Yadav, P. Chauhan, Estimation of lattice strain in Mn-doped ZnO nanoparticles and its effect on structural and optical properties, Indian J. Pure Appl. Phy. 57 (2019) 881–890.
[35] U. Seetawan, S. Jugsujinda, T. Seetawan, A. Ratchasin, C. Euvananont, C. Junin, C. Thanachayanont, P. Chainaronk, Effect of Calcinations Temperature on Crystallography and Nanoparticles in ZnO Disk, MSA. 02 (2011) 1302–1306, https://doi.org/10.4236/msa.2011.29176.
[36] P.M. Kibasomba, S. Dhlamini, M. Maaza, C.-P. Liu, M.M. Rashad, D.A. Rayan, B. W. Mwakikunga, Strain and grain size of TiO_2 nanoparticles from TEM, Raman spectroscopy and XRD: The revisiting of the Williamson-Hall plot method, Results in Physics. 9 (2018) 628–635, https://doi.org/10.1016/j.rinp.2018.03.008.
[37] S.C. Das, R.J. Green, J. Podder, T.Z. Regier, G.S. Chang, A. Moewes, Band Gap Tuning in ZnO Through Ni Doping via Spray Pyrolysis, J. Phys. Chem. C. 117 (2013) 12745–12753, https://doi.org/10.1021/jp3126329.
[38] R. Priya, P. Sahay, N. Saxena, P. Rajput, V. Chawla, R. Sharma, O.P. Sinha, R. Krishna, Systematic study of Ni, Cu co-doped ZnO nanoparticles for UV photodetector application, J Mater Sci: Mater Electron. 32 (2021) 2011–2025, https://doi.org/10.1007/s10854-020-04968-2.
[39] A.A. Ansari, A.K. Parchur, M. Alam, A. Azzeer, Effect of surface coating on optical properties of Eu^{3+}-doped $CaMoO_4$ nanoparticles, Spectrochimica Acta Part A: Molecular and Biomolecular Spectroscopy. 131 (2014) 30–36, https://doi.org/10.1016/j.saa.2014.04.036.
[40] B.P. Singh, A.K. Parchur, R.S. Ningthoujam, A.A. Ansari, P. Singh, S.B. Rai, Enhanced photoluminescence in CaMoO4:Eu^{3+} by Gd^{3+} co-doping, Dalton Trans. 43 (2014) 4779, https://doi.org/10.1039/c3dt53408a.
[41] K. Raja, P.S. Ramesh, D. Geetha, Synthesis, structural and optical properties of ZnO and Ni-doped ZnO hexagonal nanorods by Co-precipitation method, Spectrochimica Acta Part A: Molecular and Biomolecular Spectroscopy. 120 (2014) 19–24, https://doi.org/10.1016/j.saa.2013.09.103.
[42] R. Saravanan, K. Santhi, N. Sivakumar, V. Narayanan, A. Stephen, Synthesis and characterization of ZnO and Ni doped ZnO nanorods by thermal decomposition method for spintronics application, Materials Characterization. 67 (2012) 10–16, https://doi.org/10.1016/j.matchar.2012.02.015.
[43] S. Suwanboon, P. Amornpitoksuk, A. Sukolrat, N. Muensit, Optical and photocatalytic properties of La-doped ZnO nanoparticles prepared via precipitation and mechanical milling method, Ceramics International. 39 (2013) 2811–2819, https://doi.org/10.1016/j.ceramint.2012.09.050.
[44] S. Bandyopadhyay, G.K. Paul, R. Roy, S.K. Sen, S. Sen, Study of structural and electrical properties of grain-boundary modified ZnO films prepared by sol–gel technique, Materials Chemistry and Physics. 74 (2002) 83–91, https://doi.org/10.1016/S0254-0584(01)00402-3.
[45] A. Bayat, A.R. Mahjoub, M.M. Amini, Synthesis of high crystalline hierarchical self-assembled $MMoO_4$ (M=Ca, Sr and Ba) super structures: Having hydrophilic surfaces and obvious red-shifted photoluminescence behavior, Materials Chemistry and Physics. 223 (2019) 583–590, https://doi.org/10.1016/j.matchemphys.2018.11.031.
[46] A.A. Bazrafshan, M. Ghaedi, S. Hajati, R. Naghiha, A. Asfaram, Synthesis of ZnO-nanorod-based materials for antibacterial, antifungal activities, DNA cleavage and efficient ultrasound-assisted dyes adsorption, Ecotoxicology and Environmental Safety. 142 (2017) 330–337, https://doi.org/10.1016/j.ecoenv.2017.04.011.
[47] A.S. Haja Hameed, C. Karthikeyan, V. Senthil Kumar, S. Kumaresan, S. Sasikumar, Effect of Mg^{2+}, Ca^{2+}, Sr^{2+} and Ba^{2+} metal ions on the antifungal activity of ZnO nanoparticles tested against Candida albicans, Materials Science and Engineering: C. 52 (2015) 171–177, https://doi.org/10.1016/j.msec.2015.03.030.
[48] S.A. Khan, S. Shahid, W. Bashir, S. Kanwal, A. Iqbal, Synthesis, characterization and evaluation of biological activities of manganese-doped zinc oxide nanoparticles, Trop. J. Pharm Res. 16 (2017) 2331–2339, https://doi.org/10.4314/tjpr.v16i10.4.
[49] H.S. Bhargav, S.D. Shastri, S.P. Poornav, K.M. Darshan, M.M. Nayak, in: Measurement of the Zone of Inhibition of an Antibiotic, IEEE, Bhimavaram, India, 2016, pp. 409–414, https://doi.org/10.1109/IACC.2016.82.